Available online at www.sciencedirect.com

SciVerse ScienceDirect

Ceramics International 39 (2013) 999–1009

CERAMICS INTERNATIONAL

www.elsevier.com/locate/ceramint

New observations in micro-pop-in issues in nanoindentation of coarse grain alumina

Manjima Bhattacharya, Riya Chakraborty, Arjun Dey[1], Ashok Kumar Mandal, Anoop Kumar Mukhopadhyay*

CSIR-Central Glass and Ceramic Research Institute, Kolkata 700032, India

Received 11 June 2012; received in revised form 5 July 2012; accepted 5 July 2012
Available online 20 July 2012

Abstract

The present experiments were focused on nanoindentation behaviour and the attendant "micro-pop-in" in a dense (~95% of theoretical) coarse-grain (~20 μm) alumina ceramic as a function of loading rate variations at three constant peak loads in the range of 10^5–10^6 μN. Based on the experimental results here we report for the first time, to the best of our knowledge, an increase in intrinsic nano scale contact resistance as well as the nanohardness with the loading rate. These observations were explained in terms of the correlation between the nanoscale plasticity and shear stress active just underneath the nanoindenter.

Keywords: Alumina; Contact deformation rate; Nanohardness; Nanoindentation

1. Introduction

Alumina, the most well known structural ceramic finds applications such as the wear-resistant inserts, biomedical implants, high strain rate impact-resistant plates, high temperature electronic components, very high end optical components and devices. Hardness is one of the most important surface mechanical properties in this connection as it defines the intrinsic contact resistance of alumina ceramics. The defects that ultimately define the mechanical integrity of a structural ceramic originate at the nanoscale of the microstructure during its service life time. Thus, the mechanical integrity of a structural ceramic like alumina in service gets determined at the nanoscale of microstructure. Therefore, the nanoscale hardness or nanohardness of alumina measured at the nanoscale of the microstructure assumes explicit importance in this regard. In spite of the wealth of literature, however, the studies on nanohardness of dense, coarse grain alumina ceramics which characteristically exhibits an R-curve behaviour are far from significant. In recent times the nanoindentation technique has emerged as a very powerful technique to characterize the nanomechanical properties of a wide variety of materials [1–5]. That is why there exists a wealth of literature on hardness of alumina measured at macro- or micro-scale [6–8] as well as at the nanoscale [9,10]. However, these measurements [7–10] are reported mostly for fine grain and/ or submicrometer grain sized alumina ceramics and reports on coarse grain alumina ceramics are really rare [6]. Interestingly alumina is capable of localized plastic deformation even under ultra-low loads used in the nanoindentation experiments [11]. The pop-in mechanisms in nanoindentation experiments are yet to be well understood [12–16]. A lot of factors can affect the initiation of pop-in e.g. nanoindentation load, nanoindenter tip radius, temperature etc., while strain and loading rate variation may [12–15] or may not [16] influence the measured value of hardness. Recently, our work demonstrated significant effect of loading rate on nanohardness of glass [17–22] and alumina [21,22]. The occurrence of the pop-in behaviour were also reported for glass [17–20], polycrystalline alumina [21,22], bulk metallic glass [23–25], sapphire [26], GaN [27] and ZnO [28]. The occurrence of pop-in has often been associated with shear

*Corresponding author. Tel.: +91 33 2473 3469/76/77/96; fax: +91 33 2473 0957.
E-mail addresses: anoopmukherjee@cgcri.res.in, mukhopadhyay.anoop@gmail.com (A. Kumar Mukhopadhyay).
[1]Present Address: Scientist, Thermal Systems Group, ISRO Satellite Centre, Vimanapura, Post, Bangalore 560 017, India.

0272-8842/$ - see front matter © 2012 Elsevier Ltd and Techna Group S.r.l. All rights reserved.
http://dx.doi.org/10.1016/j.ceramint.2012.07.020

localization [17–33]. However, there are many contradictory view points about their genesis in a wide variety of materials [33–38] and an unequivocal picture is yet to emerge. Therefore, the major objective of the present work was to study in detail the role of *"micro-pop-in"* issues in influencing the loading rate dependence of the nanoindentation response and in particular, the nanoscale contact deformation resistance of a high density (~95% of theoretical) coarse grain (~20 μm) alumina ceramic.

2. Materials and methods

Alumina discs of ~10 mm diameter and ~3 mm thickness were prepared by pressureless sintering in air at a temperature of 1600 °C. The density of the sintered alumina discs was measured by Archimedes's principle. The polished alumina discs had surface roughness (R_a) of 0.01 μm. The polished alumina discs were thermally etched for 1 h. in air at a temperature of 1500 °C. The photomicrographs of the thermally etched alumina discs were taken using a Field Emission Scanning Electron Microscope (FE-SEM, Supra VP35, Carl Zeiss, Germany). These photomicrographs were used to measure the average grain size of the pressureless sintered alumina by an image analyzer (Q500MC, Leica, UK).

The load controlled nanoindentation technique was used in a commercial nanoindentation machine (Fischerscope H100-XYp; Fischer, Switzerland) to evaluate the nanohardness and Young's modulus of the alumina samples. A 5×5 array matrix was utilized for this purpose. The machine had depth sensing resolution of 1 nm. The load sensing resolution of the machine was 0.2 μN. The nanoindentation experiments were conducted with a Berkovich indenter attached to the machine. The indenter had a tip radius of ~150 nm and a semi-apex angle of 65.3°. The area function of the indenter tip was evaluated prior to each experiment. The dedicated software available in the control system of the machine corrected the experimentally obtained load (P) versus depth of penetration (h) data for tip blunting effect. Following the DIN 50359-1 standard the machine was finally calibrated with nanoindentation based independent evaluation of nanohardness, H (4.14 GPa) and Young's modulus, E (84.6 GPa) values of a reference BK7 glass block (Schott, Germany). The standard reference glass block was provided by the supplier of the machine. The calibration was repeated before each and every experiment to make sure that the data generated remains reproducible. Next, the Oliver-Pharr model [33] was used to measure the nanohardness and Young's modulus data of the alumina samples from the experimentally measured load-depth (P-h) data plots. No particular bias was associated with the location selection for the positions of the nanoindentation arrays. Thus, at least 25 individual measurements of nanohardness values were used for each reported average data. In the present experiments, three different constant peak loads of 10^5, 5×10^5 and 10^6 μN were used. Further, both the loading and the unloading times were varied from 10^0 to 10^3 s to obtain the variation of loading rates in the range of 10^3–10^6 μN s^{-1}. Thus, the loading rate was calculated by dividing the peak load by the time to reach the peak load. For instance a loading time of 1 s to reach a peak load of 10^3 μN gives the loading rate of 10^3 μN s^{-1}. The error bars represent ± 1 standard deviation of the data for all experimental data reported in this work. The Field Emission Scanning Electron Microscope (FE-SEM, Supra VP35, Carl Zeiss, Germany) as mentioned earlier was also used to observe the microstructure and the nanoindents in the present alumina samples.

3. Results

The two most relevant experimental data of major concern in the present work are the instantaneous depth (h) and the reduced depth (h') of penetrations recorded during the nanoindentation experiments. Here $h'\,(=h-h_f)$ is called the reduced depth of penetration following [33]. The quantity h_f represents the final depth of penetration. The experimental data on load (P) versus depth of penetration (h) are shown in Fig. 1a. The exploded view of the same data is shown in Fig. 1b. These data confirmed that a large number of serrations occurred during the loading and unloading cycles. The very presence of these

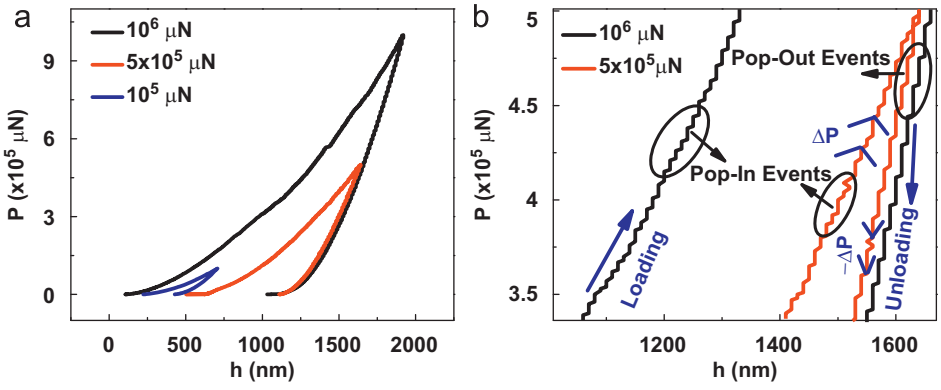

Fig. 1. (a) Load-depth plots at 3 different loads of 10^5 μN, 5×10^5 μN and 10^6 μN (b) Exploded views of Fig. 1(a).

serrations in the P-h data signify the occurrence of nanoscale plasticity events e.g. multiple micro pop-in and micro pop-out events. Both h and h' had power law dependencies on the nanoindentation load (P), Fig. 2a. Further, the rate of change of depths dh/dt and dh'/dt with respect to time was minimal i.e. constant (Fig. 2b).

The data plotted in Fig. 3(a) show the variation of depth increment (Δh) during the loading cycles as a function of the loading rate $\dot{P}$. The depth increment basically represents the change in depth between two consecutive nanoscale plasticity events (say, 1, 2) those had occurred during the loading cycles. Similarly, the data plotted in Fig. 3(b) show the variation of depth decrement ($-\Delta h$) during the unloading cycles as a function of the loading rate$\dot{P}$. The depth decrement stands for the change in depth between two consecutive nanoscale plasticity events (say, 1, 2) those had occurred during the unloading cycles. It is interesting to note that both of these data (Fig. 3a and b) exhibit power law dependencies on the loading rate $\dot{P}$. The exponents of such dependencies were positive (Fig. 3a and b). A similar trend was found for the data on the reduced depth of penetration (h'), Fig. 4.

Most interestingly, the data plotted in Fig. 5(a) show that for any given peak loads, the critical load (P_c) had power law dependence with positive exponent on the loading rate $\dot{P}$. Physically, the critical load (P_c) represents the load at and above which a nanoscale plasticity event can just initiate. In other words it signifies the intrinsic contact deformation resistance of the present alumina ceramic. This data confirmed that the critical load for initiation of plasticity at the nanoscale of the present alumina increased with loading rate. Thus, to the best of our knowledge this is the very first experimental observation that for any given peak loads during the nanoindentation experiments, the intrinsic contact deformation resistance of coarse grain alumina ceramics can increase with the loading rate.

Similarly, the data plotted in Fig. 5(b) show that for any given peak loads during the nanoindentation experiments, the maximum shear stress (τ_{max}) active just underneath the

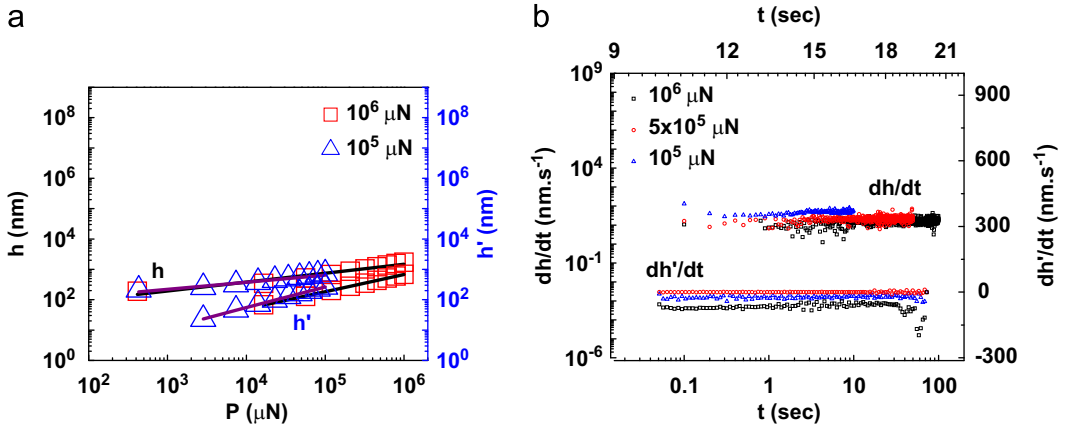

Fig. 2. (a) The experimental data on dependence of the nanoindentation depth (h) and instantaneous reduced nanoindentation depth (h') on the instantaneous nanoindentation load (P) obtained during the loading and unloading cycles respectively. The solid lines indicate the corresponding power law fits. (b) The minimal dependence of $\left(\frac{dh}{dt}\right)$ and $\left(\frac{dh'}{dt}\right)$ on time (t).

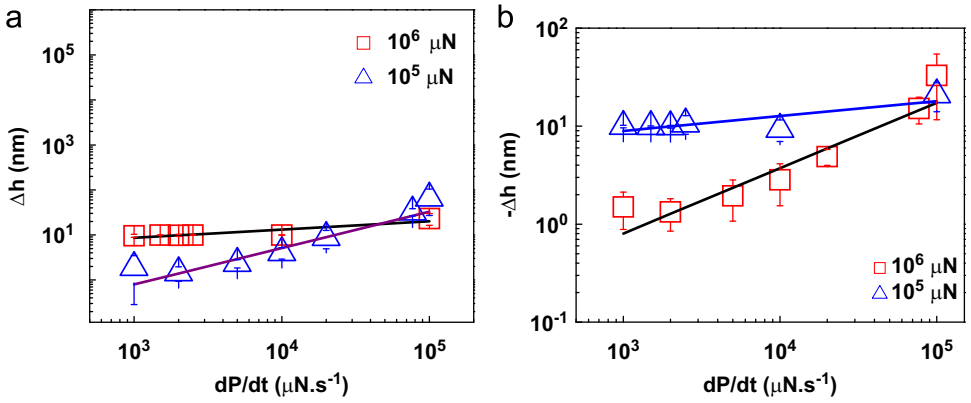

Fig. 3. The dependencies of the depth increment (Δh)$=h_{c2}-h_{c1}$ (at which two consecutive nanoscale plasticity events say, 1 and 2 had occurred) and (b) depth decrement ($-\Delta h$)$=h_{c1}-h_{c2}$ on the loading rates $\left(\frac{dP}{dt}\right)$. The hollow rectangle and triangle represent respectively Δh and $-\Delta h$ at 10^6 μN and 10^5 μN loads. The solid lines indicate the corresponding power law fits.

nanoindenter had a power law dependence with positive exponent on the loading rate, $\dot{P}$. The magnitudes of (τ_{max}) were estimated following [29,30].

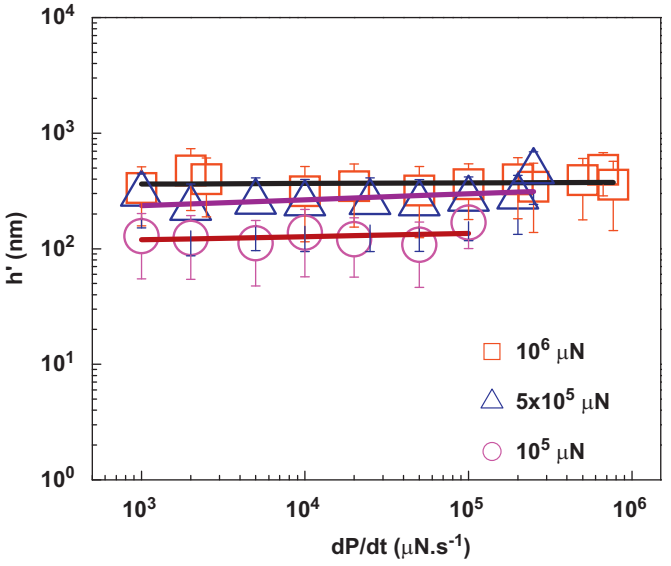

Fig. 4. The dependencies of instantaneous reduced nanoindentation depth (h') on the loading rates ($\frac{dP}{dt}$) at 3 different loads of 10^5 μN, 5×10^5 μN and 10^6 μN. The solid lines indicate the corresponding power law fits.

FE-SEM photomicrographs of the nanoindentation cavities are presented in Fig. 6a and b. These photomicrographs show distinct evidence for presence of shear induced localized microcracking in the vicinity of the nanoindent and micro-shear band formation inside the nanoindentation cavity.

The depth (h_c) recorded corresponding to the critical load (P_c) is called the critical depth of penetration. Thus, $\Delta h(=h_{c2}-h_{c1})$ represents the change in critical depth data between the occurrences of two nanoscale plasticity events in the present alumina ceramic sample. Further, the corresponding load increment $\Delta P(=P_{c2}-P_{c1})$ represents the change in critical load data between the occurrences of two nanoscale plasticity events. The data presented in Fig. 7 show that for any given peak loads during the nanoindentation experiments h_c had empirical power law dependence on P_c. Similarly, the data plotted in Fig. 8 demonstrate that Δh had power law dependence on P_c. Further, Δh had also an empirical power law dependence on the corresponding load increment ΔP, Fig. 9.

The data on variation of the final penetration depth (h_f) as a function of the loading rate, $\dot{P}$ are shown in Fig. 10. The final penetration depth values were relatively larger at comparatively lower loading rates and smaller at comparatively higher loading rates.

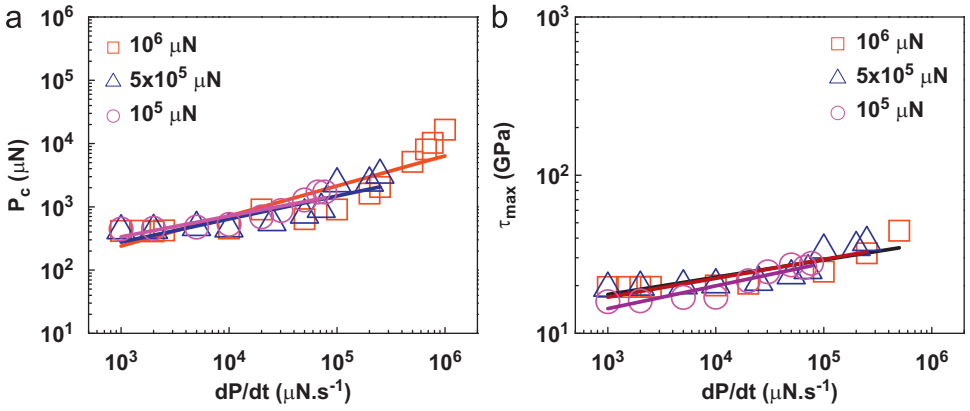

Fig. 5. Variation of (a) the critical load (P_c) and (b) the maximum shear stress (τ_{max}) active just underneath the nanoindenter as a function of the loading rates ($\frac{dP}{dt}$). The solid lines indicate the corresponding power law fits.

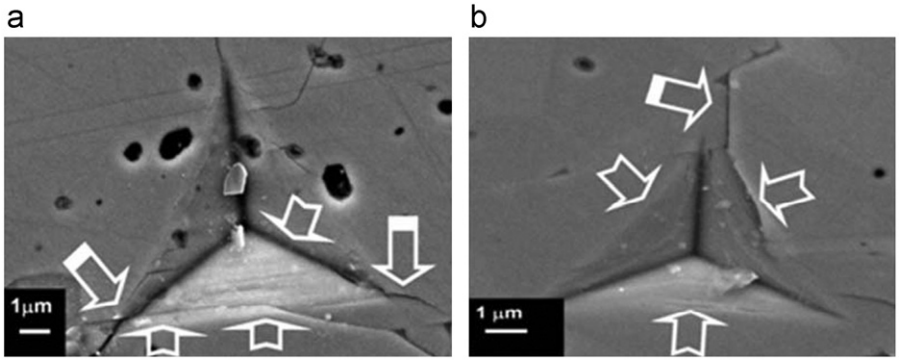

Fig. 6. FESEM photomicrographs of shear induced deformation band formation and microcracking (marked by hollow white arrows) at the nanoindentation cavities of alumina at typical illustrative lower loading rates of (a) 2×10^3 and (b) 10^6 μN s^{-1}.

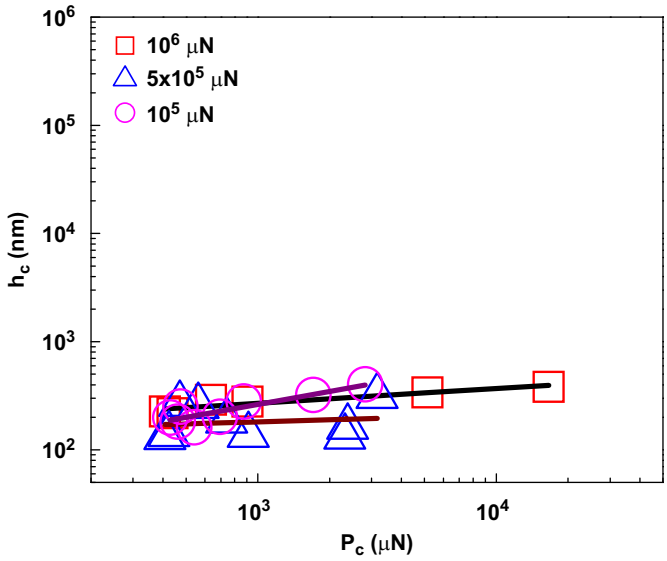

Fig. 7. The dependencies of the critical depth (h_c) on the critical load (P_c). The solid lines indicate the power law fits.

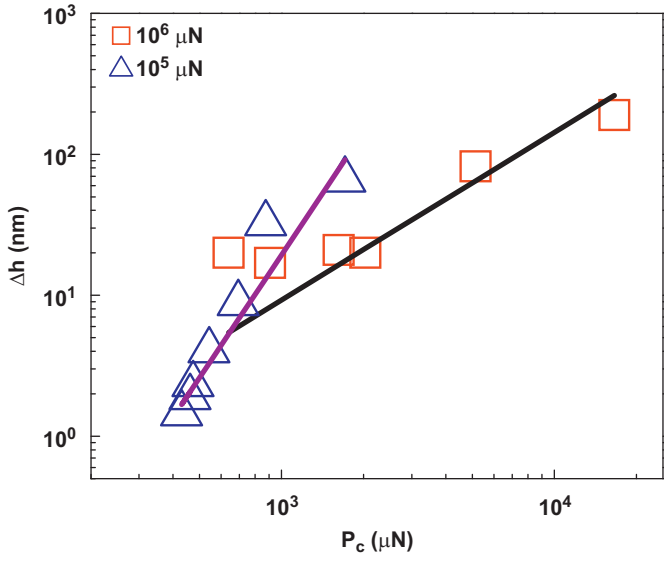

Fig. 8. The dependencies of the depth increment $\Delta h = h_{c2} - h_{c1}$ (at which two consecutive nanoscale plasticity events say, 1 and 2 had occurred) on the critical load (P_c). The solid lines indicate the corresponding power law fits.

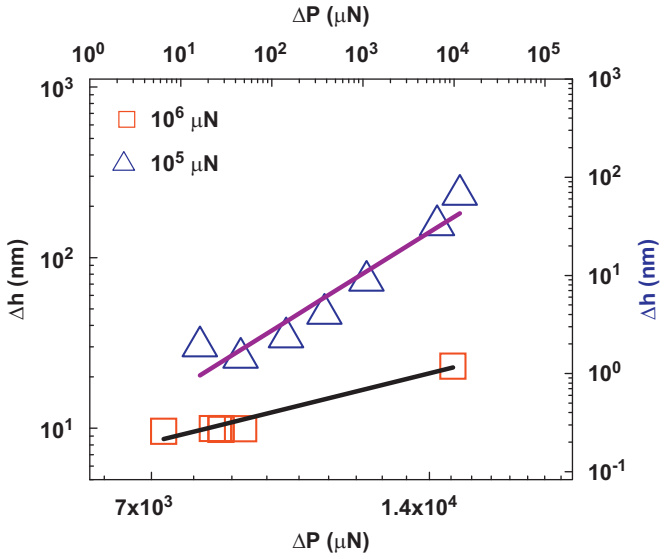

Fig. 9. The dependence of depth increment $\Delta h = h_{c2} - h_{c1}$ on the corresponding load increment $\Delta P = P_{c2} - P_{c1}$ at which two consecutive nanoscale plasticity events (say, 1, 2) had occurred during the loading cycles for 10^5 and 10^6 μN peak loads. The solid lines indicate the corresponding power law fits.

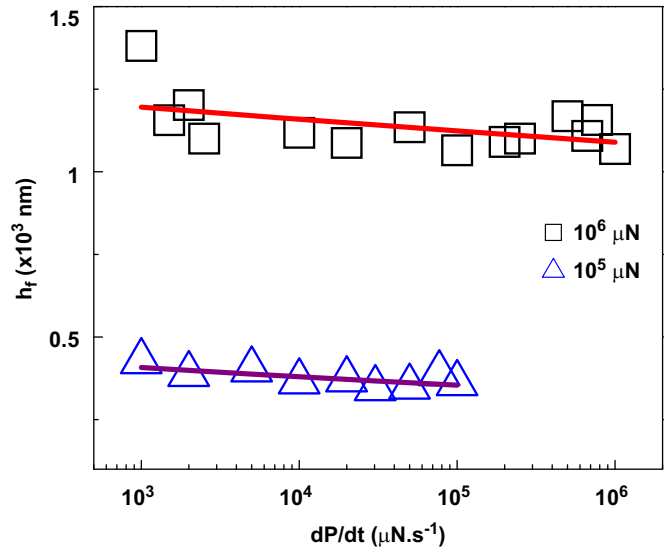

Fig. 10. Variation of the final depth of penetration (h_f) as a function of loading rates ($\frac{dP}{dt}$) for 10^5 and 10^6 μN peak loads. The solid lines indicate the corresponding power law fits.

Finally, the data on variation of the nanohardness (H) are presented in Fig. 11 as a function of the loading rate $\dot{P}$. The data show that for any given peak loads during the present nanoindentation experiments, the nanohardness (H) increased with loading rate, Fig. 11. To the best of our knowledge this is also the very first observation that the nanohardness of coarse grain alumina can register an apparent increase with loading rate. However, the data on variation of the Young's modulus, E as a function of the loading rate, $\dot{P}$ (Fig. 12) show that it was insensitive to the variations in loading rate, as expected.

4. Discussions

Before discussing the experimental data it should be recognized that so far, the issue of pop-in behavior in nanoindentation work of a wide variety of materials has not received appreciable theoretical framework of investigation [26–38]. However, many authors have argued that pop-in signifies the initiation of nanoscale plasticity events in a given material [27–35]. Therefore, an attempt was made to develop a simplistic theoretical scenario and then

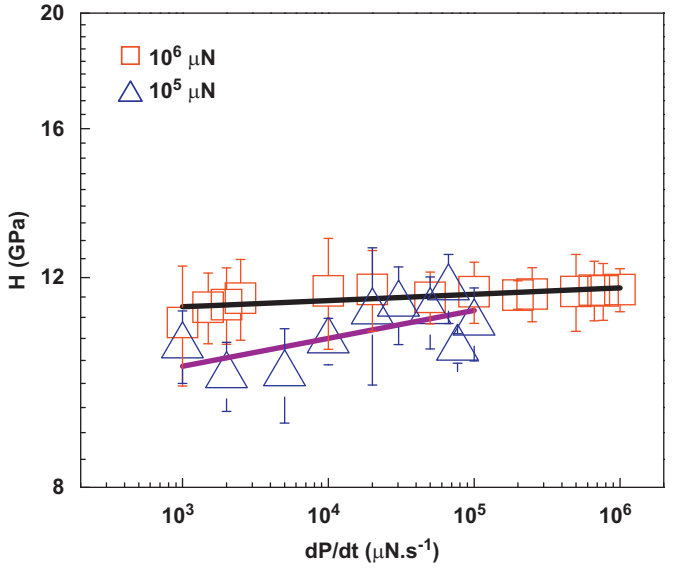

Fig. 11. Variations of nanohardness as a function of loading rates $\left(\frac{dP}{dt}\right)$ at the peak loads of 10^5, 5×10^5 and 10^6 μN. The solid lines indicate the corresponding power law fits.

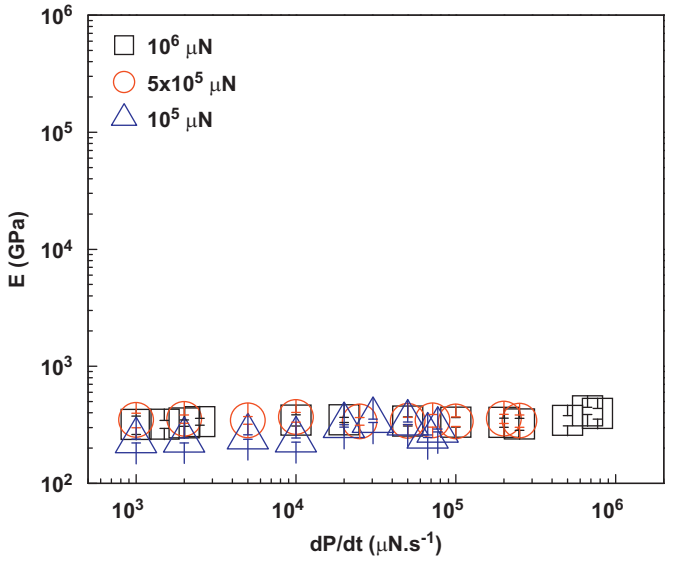

Fig. 12. Variations of Young's modulus as a function of loading rates $\left(\frac{dP}{dt}\right)$ at the peak loads of 10^5, 5×10^5 and 10^6 μN.

examine whether that scenario was in accordance with the present experimental data.

According to [38], the instantaneous nanoindentation depth (h) is related to the corresponding instantaneous load (P) by:

$$P = Bh^m \tag{1}$$

where B and m are empirical constants and generally, $1 < m \leq 2$ [38]. We note that from Eq. (1) above we can get:

$$h = \left(B^{-1}\right)^{\left(\frac{1}{m}\right)}(P)^{\left(\frac{1}{m}\right)} = AP^n \tag{2}$$

where $A = \left(B^{-1}\right)^{\left(\frac{1}{m}\right)}$ and $n=(1/m)$ are empirical constants. It has been shown by us elsewhere [22] that one can obtain the following relationship from Eq. (1) above by differentiating both sides with respect to time (t):

$$\dot{P} = Bmh^{m-1}\dot{h} \tag{3}$$

Eq. (3) can be re-written as:

$$h = C\dot{P}^{\alpha} \tag{4}$$

In Eq. (4), the quantities C and α are given by:

$$C = \left(Bm\dot{h}\right)^{-\alpha} \tag{5}$$

and

$$\alpha = \frac{1}{(m-1)} \tag{6}$$

From Eq. (5) it follows that the quantity C becomes a constant if $\dot{h}$ is a constant, because the quantities B and m are already defined as constants. If C is a constant it follows automatically from Eq. (4) that

$$h \propto \dot{P}^{\alpha} \tag{7}$$

The empirical relationship proposed by Oliver and Pharr [33] is that during the unloading cycles:

$$P = Ah'^{\beta} \tag{8}$$

Using treatment similar to what has been done above; Eq. (8) can be easily cast as:

$$h' = GP^{\lambda} \tag{9}$$

where G and λ are empirical constants. Following the similar type of mathematical manipulations as done for Eqs. (3)–(7), Eq. (9) could be also recast as:

$$h' \propto \dot{P}^{\zeta} \tag{10}$$

Thus, Eq. (10) is of the similar form as of Eq. (7). In Eq. (10) ζ is an appropriate constant that could be defined in a manner similar to how the constant α was defined above. Table 1 gives a summary of the pre-exponential and exponential factors those were obtained by fitting of the corresponding data from the present work to the Eqs. (2), (4), (9) and (10). The general trend was that with increase in load the pre-exponential factors increased while the corresponding exponents decreased.

The experimental data plotted in Figs. 3(a, b) and 4 show that (Δh) and ($-\Delta h$) as well as the reduced depth of penetration (h'), had power law dependencies on the loading rate $\dot{P}$. This is in accordance with the predictions of Eqs. (7) and (10) deduced above. This match between the experimental data and predicted trend occurred for two reasons. Firstly, as proposed in the theoretical framework e.g. Eqs. (2) and (9); both h and h' had power law dependencies on the nanoindentation load (P), Fig. 2a. Secondly, the rates of change of depths dh/dt and dh'/dt were constant with respect to time, Fig. 2b.

It is interesting to note that the data of (Δh) as given in Ref. [31] also showed a power law variation with the loading rate $\dot{P}$ that spanned a range of 50–400 μN s^{-1}.

Table 1
Summary of the pre-exponential and exponential factors obtained by fitting the relevant data from the present work to Eqs. (2), (4), (9) and (10).

P (μN)	10^5	10^6
Values of the power law exponents (n, λ, α, ε, v) and the pre-exponential factors (A, B, C, G)		
h vs. P cf. Eq.(2)	$A=43.15$, $n=0.23$	$A=25.4$, $n=0.3$
h' vs. P cf. Eq.(9)	$G=0.105$, $\lambda=0.68$	$G=0.26$, $\lambda=0.57$
Δh vs. dP/dt cf. Eq. (4)	$C=0.0036$, $\alpha=0.81$	$C=2.504$, $\alpha=0.18$
$(-\Delta h)$ vs. dP/dt cf. Eq. (4)	$C=0.008$, $\alpha=0.67$	$C=3.13$, $\alpha=0.15$
h' vs. dP/dt cf. Eq. (10)	$D=98.6$, $\zeta=0.027$	$D=350.5$, $\zeta=0.005$
h_c vs. P_c cf. Eq. (2)	$A=17$, $n=0.4$	$A=106$, $n=0.13$
Δh vs. P_c cf. Eq. (2)	$A=4\times10^{-8}$, $n=2.9$	$A=0.08$, $n=0.79$
Δh vs. ΔP cf. Eq. (2)	$A=0.19$, $n=0.58$	$A=0.6\times10^{-4}$, $n=1.33$
h_f vs. dP/dt cf. eq. (4)	$C=503.67$, $\alpha=-0.03$	$C=1312.6$, $\alpha=-0.01$

However, the authors did not explicitly discussed about any such dependence in Ref. [31]. Fitting of the experimental data from [31] to our proposed Eq. (4) yields:

$$\Delta h = 6.5\left(\frac{dP}{dt}\right)^{0.09} \tag{11}$$

It is worth mentioning that although the materials and the experimental conditions of the present work were different from those reported in [31], the values of the pre-exponential and exponential factors of Eq. (11) had at least an order of magnitude match with the values (e.g., $C=2.504$, $\alpha=0.18$, peak load 10^6 μN, loading rate 10^3–10^6 μN s^{-1}) obtained in the present work (Table 1). Thus, the data from literature [31] also exhibited a trend that was similar to what has been observed (Fig. 3a) in the present work.

A large number of serrations occurred during the loading and unloading cycles signifying the presence of nanoscale plasticity e.g. multiple micro pop-in and micro pop-out events (Fig. 1a and b). As mentioned earlier, this kind of behaviour was also reported for glass [17–20], polycrystalline alumina [21,22], bulk metallic glasses [23–25], sapphire [26], GaN [27] and ZnO [28]. The genesis of such nanoscale plasticity events has been correlated [17–28] to shear burst and shear localization that initiates at a critical load (P_c).

Most interestingly, for any given peak loads during the present nanoindentation experiments, the intrinsic contact deformation resistance i.e. the critical load (P_c) for initiation of nanoscale plasticity events in the present coarse grain alumina exhibited power law dependence: $P_c = 8.97\left(\frac{dP}{dt}\right)^{0.48}$ on the loading rate, Fig. 5(a). This happens because at higher loading rate, the rate of energy transfer is much quicker compared to that at lower loading rate. Therefore, it leads to more localized compressive strain generation. Since the Young's moduli data were insensitive to variations in $\dot{P}$ (Fig. 12); this higher compressive strain leads to a higher compressive stress. Thus, at higher loading rates a higher critical load is required to overcome this localized compressive stress to initiate afresh the plasticity events at the nanoscale e.g. shear induced microcracking and/or shear band formation [31,32]. In fact such a picture is totally supported by the FE-SEM based evidence of shear induced localized microcracking in the vicinity of the nanoindent and micro-shear band formation inside the nanoindentation cavity, Fig. 6a and b.

It is interesting to note that although not explicitly mentioned by the authors the data of (P_c) as given in Ref. [31] had a power law dependence on the loading rate $\dot{P}$ that spanned the range of 50–400 μN s^{-1}. Fitting of the data of P_c from Ref. [31] to the loading rate yields:

$$P_c = 1.36\left(\frac{dP}{dt}\right)^{0.07} \tag{12}$$

It is worth mentioning that the materials and the experimental conditions were different between Ref. [31] and the present work. Even then there was an order of magnitude match between the values of the pre-exponential and exponential factors of Eq. (12) with the values (pre-exponential factor 8.97, exponential factor 0.48, peak load 10^6 μN, loading rate 10^3–10^6 μN s^{-1}) obtained in the present work. Thus, the data from literature [31] also followed a trend that was similar to that of the present work.

The maximum shear stress (τ_{max}) active underneath the nanoindenter showed a similar power law dependence on the loading rate, ($\dot{P}$), Fig. 5(b). The reason for this is that it was directly dependent on the critical load (P_c) as [29,30]:

$$\tau_{max} = 0.4459\left(\frac{16P_cE_r^2}{9\pi^3}R^2\right)^{1/3}$$

It may be mentioned that the estimated maximum shear stress (τ_{max}) active just underneath the nanoindenter (e.g. ~10–20 GPa, Fig. 5b) was much greater than the theoretical shear strength (e.g., 3 GPa) of alumina [6]. Hence, shear induced deformation and/or localized micro-fracture was expected, Fig. 6a and b.

For any given peak load both h_c (Fig. 7) and Δh (Fig. 8) had power law dependencies on P_c. These observations were again in accordance with the trend proposed by Eq. (2). It was also found out that the data of (Δh) as given in Ref. [31] had a power law dependence on the critical load P_c. Fitting of the relevant data from Ref. [31] to our proposed Eq. (2) yields:

$$\Delta h = 5.08(P_c)^{0.54} \tag{13}$$

The materials and the experimental conditions were not exactly the same between the present work and those reported in Ref. [31]. In spite of that difference there was an order of magnitude match between the values of the pre-exponential and exponential factors of Eq. (13) with the values ($A=0.08$, $n=0.79$ from Eq. (2), Table 1) obtained from the present work. Therefore, it may be argued that the data from literature [31] also followed a trend that was similar to that of the present work.

Further, Δh had power law dependence on ΔP, Fig. 9.This was in accordance with the trend proposed by Eq. (2) mentioned above. As a matter of fact it is interesting to note that the data obtained at a loading rate of 31000 $\mu N\,s^{-1}$ from [37] had a similar power law dependence given by:

$$\Delta h = 10^{-4}(\Delta P)^{1.4} \quad (14)$$

In spite of the difference between materials and the experimental conditions between those reported in Ref. [37] and the present work, the pre-exponential factor and exponent values of Eq. (14) had an order of magnitude match with the values ($A=0.6\times10^{-4}$, $n=1.33$ from Eq. (2), Table 1) obtained at a peak load of 10^6 μN used in the present work.

Because the nanoscale contact resistance increased with the loading rate, at lower values of $\dot{P}$, the final penetration depth (h_f) will be of higher magnitude but it will register comparatively lower magnitudes at higher loading rates. The data presented in Fig. 10 supports this qualitative picture. As h_f decreases so does the projected contact area A_c. Since the nanohardness (H) is calculated as P/Ac, [33] it therefore follows from the data of Fig. 10 why for any given peak load, the nanohardness (H) of the present coarse grain alumina ceramic increased with loading rate, Fig. 11.

To the best of our knowledge this is also the *very first experimental observation* that the nanohardness of coarse grain alumina can register an apparent increase with loading rate. It still remains to elucidate the genesis and role of the experimentally observed "*micro-pop-in*" behaviours in the nanoscale contact deformation behaviour of alumina.

Although excellent reviews are available on the nanoindentation behaviour of bulk metallic glasses [BMG], quasicrystals, glasses, metals, single and polycrystalline ceramics, ceramic thin films, coatings and semiconductors [39,40]; as is shown below [40–62], the genesis of the "*micro-pop-in*" phenomenon is yet to be fully understood, especially in ceramics. Therefore it is plausible to believe that a discussion on the deformation processes associated with the pop-in behavior of different materials might illuminate better the physics of deformation of the present alumina ceramics at the nanoscale.

The presence of pop-in has been observed by many researchers in BMG. The occurrence of pop-in in BMGs has been attributed to the discrete emission of shear bands, more so at lower loading rates than at higher loading rates [40–43]. A cooperative shearing model was also recently used to estimate the size of shear transformation zone in a BMG in connection with the statistical analysis of the "pop-in" events [44].

The first pop-in in *quasicrystals* was proposed to correspond to the maximum shear stress required to activate slip [45]. The genesis of pop-in events in the case of soda lime silica glass are governed by the positions of local weakness provided by the network modifiers [17–20]. Therefore, in BMGs and quasicrystals the pop-in occur mainly by discrete emission of shear bands and activation of the maximum shear stress condition while in glass it may be linked to changes in the short range atomic arrangements at positions of network modifiers [17–20,39–45].

Pop-in events in bulk, pure Au and Pt have been associated with homogeneous nucleation of dislocation loops beneath the nanoindentation and a heterogeneous dislocation nucleation process induced by dislocation source activation or multiplication [46]. The additional pop-in events at higher loads in Pt were associated with further dislocation motion, multiplication, and the evolution of a complex defect structure [46]. In Al thin films and single crystal Al pop-in occurred when the maximum shear stress underneath the nanoindenter, which was of the order of the theoretical shear strength, triggered displacement bursts by the nucleation of dislocations [36]. In contrast, for bulk aluminium a combination of electron channeling contrast imaging and nanoindentation tests confirmed that a very low dislocation density is necessary to observe the pop-in [47]. Very recent in situ nanoindentation on Fe-3 wt%Si single crystal inside a transmission electron microscope showed that dislocations formed during the early stage involved not distinguishable pop-ins but small load fluctuations and the actual pop-in behavior was connected with the change of dislocation structures [48,49]. Slip rate dependent friction can also act as a potential contributor to pop-in during the nanoindentation of nickel [50]. Hence, the main factors affecting the pop-in behavior of metallic materials seemed to be the load, the loading rate as well as the generation, amount, change of structure, movement, arrest and repeated movement of dislocations apart from the slip rate dependence of interfacial friction [36,46–50].

The "pop-in" behavior in single and polycrystalline alumina ceramics were linked to rhombohedral twinning activated under a penetrating nanoindenter, dislocation movement across slip planes and nucleation of homogeneous dislocations when the theoretical shear strength is exceeded [26,31,32]. However, for single crystal HAP "pop-in" behaviour was associated to presence of microcrack, a pore underneath the indenter, or the pile-up phenomenon [51]. The pop-in events in ZnO single crystal was claimed to be due to the initiation of slip [28]. Slip by punching out of dislocation bands parallel to the basal planes was the reason for pop-in in GaN epilayers [27] but pop-ins happened due to dislocation loop multiplication and their movement from plane to plane by cross-slip in c-plane of GaN [52]. The ZrB_2 ceramics exhibited pop-in

due to homogeneous dislocation nucleation [53]. However, microcracks in the pore wall were thought to cause pop-in in silica aerogels [54]. Therefore, activation of rhombohedral twinning, initiation of slip due to nucleation of homogeneous dislocations and their movement across slip planes as well as slip by punching out of dislocation bands parallel to specific crystallographic planes, dislocation loop multiplication followed by movement from plane to plane by cross-slip, and presence of pores and/or microcracks underneath the nanoindenter are believed to be the major causes of pop-in behavior in ceramics [26,27,31,32,51–54].

The pop-in in Si happens due to the onset of phase transition [55]. However, the random pop-in behavior in GaAs epitaxial layers was due to the random distance of pre-existing defects from the indent location [56]. In amorphous ZrCuTi/PdCuSi nanolaminates pop-in was linked to the formation of shear localization as in BMGs [57]. In multilayered epitaxial $YBa_2Cu_3O_{7-\delta}$ thin films and coated conductors pop-in was attributed to a change of crack morphology [58]. Hence, applied loads and loading rates, the onset of pressure induced phase transition, shear localization, and the presence of defects and/or cracks and their morphology at prospective locations are thought to be the main reasons of pop-in in semiconductors and thin films [55–58].

Similarly pop-in in nano-size nickel grains embedded in a carbonaceous matrix happened due to defects such as grain boundaries in the heterogeneous films [59]. The cracking and delamination of the Ni/Au coating from the acrylic core was linked to pop-in in Ni/Au nano-coated acrylic particles [60]. The intergranular brittle fracture of the Ni film caused pop-in in ultra thin Ni films on sapphire [61]. But dislocation interaction was thought to cause pop-in in compositionally graded $Ti_{1-x}Al_xN$ multilayer thin films [62]. Therefore, the grain boundary defects, cracking and coating delamination at the interface as well as dislocation interaction caused pop-in in nanocrystalline materials, coatings and multilayered structures [59–62].

In the light of the foregoing discussions at P_c when the first "*micro pop-in*" event initiates, the nanoindenter is just supported by the surrounding microstructure which is under huge compressive contact stress as well as shear stress operative at the vicinity of the tip. It is suggested that the initiation of first "*micro pop-in*" event, if related to localized microcrack generation; can create a local relaxation of the surrounding microstructure [63]. This process not only aids in partially releasing the strain but also reduces the local load bearing contact area. Therefore, this step is followed by a small increase in nanoscale depth at P_c. It can happen because over the small time scale involved there is an instantaneous decrease in the available load bearing contact area between the penetrating nanoindenter and the surrounding microstructure at the tip of it. As a consequence, the local compressive stress into the microstructure is momentarily enhanced leading thereby to further displacement of the microstructure by the nanoindneter. As the depth of contact increases, so does the load bearing contact area. This event causes a local drop of the compressive stress. For initiation of the second "*micro pop-in*" event, therefore, the stress has to be higher than that at the immediate previous level. This can only happen if there is a minute increase in load for the same load bearing contact area. As soon as the second micro pop-in event happens, the similar cycle of events as mentioned above follow sequentially. This is how the series of "*micro pop-in*" events as shown in Fig. 1b can happen.

As far as the "*micro pop-out* events" are concerned it is guessed that these may be due to new, additional microcracking generated during the unloading cycle or due to localized growth of the existing microcracks during the unloading cycle. Further experimentation would be necessary to confirm this conjecture.

5. Conclusions

To the best of our knowledge, the present work is the very first experimental observation that in the case of a high density (95% of theoretical) coarse grain (~20 μm) alumina ceramic undergoing nanoindentation at three different constant peak loads of 10^5 μN, 5×10^5 μN and 10^6 μN, the intrinsic contact resistance i.e. the critical load (P_c) against the initiation of nanoscale plasticity events can enhance with the loading rate following a power law dependence with a positive exponent. Also, for the very first time to the best of our knowledge here we report the experimental observation that the nanohardness of the present coarse grain alumina ceramic can register an apparent increase with the increase in loading rate. These and the related observations were explained by a model described in the present work and the estimations of the maximum shear stress generated just underneath the nanoindenter.

Acknowledgements

The authors are grateful to the Director, CSIR-Central Glass and Ceramic Research Institute (CGCRI), Kolkata for his kind permission to publish this paper. In addition, the authors appreciate the infrastructural supports received from all colleagues and particularly those received from the colleagues of the Mechanical Property Evaluation Section, NOCCD. Finally, the authors gratefully acknowledge the financial supports received from CSIR (Project no. NWP 0027, NWP 0029).

References

[1] C.Y. Tang, P.S. Uskokovic, C.P. Tsui, Dj. Veljovic, R. Petrovic, Dj. Janackovic, Influence of microstructure and phase composition on the nanoindentation characterization of bioceramic materials based on hydroxyapatite, Ceramics International 35 (2009) 2171–2178.

[2] A. Dey, A.K. Mukhopadhyay, S. Gangadharan, M.K. Sinha, D. Basu, N.R. Bandyopadhyay, Nanoindentation study of microplasma sprayed hydroxyapatite coating, Ceramics International 35 (2009) 2295–2304.

[3] Kaimin Shih Yue He, Nano-indentation on nickel aluminate spinel and the influence of acid and alkaline attacks on the spinel surface, Ceramics International 38 (2012) 3121–3128.
[4] S. Ghosh, R. Chakraborty, N. Dandapat, K.S. Pal, S. Datta, D. Basu, Characterization of alumina–alumina/graphite/monel superalloy brazed joints, Ceramics International 38 (2012) 663–670.
[5] J.J. Roa, B. Gastoń-García, E. García-Lecina, C. Müller, Mechanical properties at nanometric scale of alumina layers formed in sulphuric acid anodizing under burning conditions, Ceramics International 38 (2012) 1627–1633.
[6] G.R. Anstis, P. Chantikul, B.R. Lawn, D.B. Marshall, A critical evaluation of indentation techniques for measuring fracture toughness: I, direct crack measurements, Journal of the American Ceramic Society 64 (1981) 533–538.
[7] A. Krell, P. Blank, Grain size dependence of hardness in dense submicron alumina, Journal of the American Ceramic Society 78 (1995) 1118–1120.
[8] A. Franco, S.G. Roberts, P.D. Warren, Fracture toughness, surface flaw sizes and flaw densities in Al_2O_3, Acta Materialia 45 (1997) 1009–1015.
[9] A. Krell, S. Schadlich, Nanoindentation hardness of submicrometer alumina ceramics, Materials Science and Engineering A 307 (2001) 172–181.
[10] A. Krell, P. Blank, H. Ma, T. Hutzler, M. Nebelung, Processing of high-density submicrometer Al_2O_3 for new applications, Journal of the American Ceramic Society 86 (2003) 546–553.
[11] L. Boudoukha, F. Halitim, S. Paletto, G. Fantozzi, Mechanical properties of titanium implanted polycrystalline Alumina and Sapphire determined by nanoindentation, Ceramics International 24 (1998) 189–198.
[12] A.G. Evans, T.R. Wilshaw, Dynamic solid particle damage in brittle materials: an appraisal, Journal of Materials Science 12 (1977) 97–116.
[13] M.M. Chaudhri, J.K. Wells, A. Stephens, Dynamic hardness, deformation and fracture of simple ionic crystals at very high rates of strain, Philosophical Magazine A 43 (1981) 643–664.
[14] D.B. Marshall, A.G. Evans, Z. Nisenholz, Measurement of dynamic hardness by controlled sharp-projectile impact, Journal of the American Ceramic Society 66 (1983) 580–585.
[15] R.J. Anton, G. Subhash, Dynamic vickers indentation of brittle materials, Wear 239 (2000) 27–35.
[16] G.D. Quinn, P.J. Patel, I. Lloyd, Effect of loading rate upon conventional ceramic microindentation hardness, Journal of Research of the National Institute of Standards and Technology 107 (2002) 299–306.
[17] R. Chakraborty, A. Dey, A.K. Mukhopadhyay, Loading rate effect on nanohardness of soda–lime–silica glass, Metallurgical and Materials Transactions A 41 (2010) 1301–1312.
[18] A. Dey, R. Chakraborty, A.K. Mukhopadhyay, Nanoindentation of soda lime–silica glass: effect of loading rate, International Journal of Applied Glass Science 2 (2011) 144–155.
[19] A. Dey, R. Chakraborty, A.K. Mukhopadhyay, Enhancement in nanohardness of soda–lime–silica glass, Journal of Non-Crystalline Solids 357 (2011) 2934–2940.
[20] R. Charkraborty, A. Dey, A.K. Mukhopadhyay, Role of the energy of plastic deformation and the effect of loading rate on nanohardness of soda–lime silica glass, Physics and Chemistry of Glasses—European Journal of Glass Science and Technology Part B 51 (2010) 293–303.
[21] M. Bhattacharya, R. Chakraborty, A. Dey, A.K. Mukhopadhyay, S.K. Biswas, Effect of Loading Rate on nano-mechanical Properties of Alumina, Workshop on Mechanical Behaviour of Systems at Small Length Scales-3, Trivandrum, India, September 18–21, 2011, p. 40 in Book of Abstracts.
[22] M. Bhattacharya, R. Chakraborty, A. Dey, A.K. Mandal, A.K. Mukhopadhyay, Applied Physics A: Materials Science and Processing, doi:10.1007/s00339-012-6888-4, in press.
[23] C.A. Schuh, T.G. Nieh, Y. Kawamura, Rate dependence of serrated flow during nanoindentation of a bulk metallic glass, Journal of Materials Research 17 (2002) 1651–1654.
[24] Y.I. Golovin, V.I. Ivolgin, V.A. Khonik, K. Kitagawa, A.I. Tyurin, Serrated plastic flow during nanoindentation of a bulk metallic glass, Scripta Materialia 45 (2001) 947–952.
[25] C.A. Schuh, T.G. Nieh, A nanoindentation study of serrated flow in bulk metallic glasses, Acta Materialia 51 (2003) 87–99.
[26] R. Nowak, T. Sekino, K. Niihara, Surface deformation of sapphire crystal, Philosophical Magazine A 74 (1996) 171–194.
[27] J.E. Bradby, S.O. Kucheyev, J.S. Williams, J.W. Leung, M.V. Swain, P. Munroe, G. Li, M.R. Phillips, Indentation-induced damage in GaN epilayers, Applied Physics Letters 80 (2002) 383–385.
[28] S.O. Kucheyev, J.E. Bradby, J.S. Williams, C. Jagadish, M.V. Swain, Mechanical deformation of single-crystal ZnO, Applied Physics Letters 80 (2002) 956.
[29] C.E. Packard, C.A. Schuh, Initiation of a shear band near a stress concentration in metallic glass, Acta Materialia 55 (2007) 5348–5358.
[30] H. Shang, T. Rouxel, M. Buckley, C. Bernard, Viscoelastic Behavior of Soda–Lime–Silica Glass Determined by High Temperature Indentation Test, Journal of Materials Research 21 (2006) 632–638.
[31] W.G. Mao, Y.G. Shen, C. Lu, Deformation behaviour and mechanical properties of poly-crystalline and single crystal alumina during nanoindentation, Scripta Materialia 65 (2011) 127–130.
[32] W.G. Mao, Y.G. Shen, C. Lu, Nanoscale elastic–plastic deformation and stress distributions of the C plane of sapphire single crystal during nanoindentation, Journal of the European Ceramic Society 31 (2011) 1865–1871.
[33] W.C. Oliver, G.M. Pharr, Measurement of hardness and elastic modulus by instrumented indentation: Advances in understanding and refinements to methodology, Journal of Materials Research 19 (2004) 3–20.
[34] H. Bei, Y.F. Gao, S. Shim, E.P. George, G.M. Pharr, Strength differences arising from homogeneous versus heterogeneous dislocation nucleation, Physical Review B 77 (2008) 060103–060107.
[35] T.F. Page, W.C. Oliver, C.J. Mchargue, The deformation- behavior of ceramic crystals subjected to very low load (nano)indentations, Journal of Materials Research 7 (1992) 450–473.
[36] A. Gouldstone, H.J. Koh, K.Y. Zeng, A.E. Giannakopoulos, S. Suresh, Discrete and continuous deformation during nanoindentation of thin films, Acta Materialia 48 (2000) 2277–2295.
[37] C.A. Schuh, A.C. Lund, Application of nucleation theory to the rate dependence of incipient plasticity during nanoindentation, Journal of Materials Research 19 (2004) 2152–2158.
[38] T. Ebisu, S. Horibe, Analysis of the indentation size effect in brittle materials from nanoindentation load–displacement curve, Journal of the European Ceramic Society 30 (2010) 2419–2426.
[39] D.A. Lucca, K. Herrman, M.J. Klofstein, Nanoindentation: Measuring methods and applications, CIR, Annals - Manufacturing Technology 59 (2010) 803–819.
[40] N.K. Mukhopadhyay, P. Paufler, Micro- and nanoindentation techniques for mechanical characterisation of materials, International Materials Review 51 (2006) 209–245.
[41] Y.I. Golovin, A.I. Tyurin, B.Y. Farber, Time-dependent characteristics of materials and micromechanisms of plastic deformation on a submicron scale by a new pulse indentation technique, Philosophical Magazine A 82 (2002) 1857–1864.
[42] N.K. Mukhopadhyay, A. Belger, P. Paufler, D.H. Kim, Nanoindentation studies Cu based bulk metallic glasses, Materials Science and Engineering A 449 (2007) 954–957.
[43] L. Zhao, C.L. Ma, M.W. Fu, X.R. Zeng, Investigation on the structural characteristics of metallic glasses based on the first displacement excursion behavior in nanoindentation, Materials Science and Engineering A 530 (2011) 196–201.
[44] I.C. Choi, Y. Zhao, B.G. Yoo, Y.J. Kim, J.Y. Suh, U. Ramamurty, J.I. Jang, Estimation of the shear transformation zone size in a bulk metallic glass through statistical analysis of the first pop-in stresses during spherical nanoindentation, Scripta Materialia, doi:10.1016/j.scriptamat.2012.02.032, in press.
[45] B. Wolf, K.O. Bambauer, P. Paufler, On the temperature dependence of the hardness of quasicrystals Materials Science and Engineering A 298 (2001) 284–295.

[46] C.A. Schuh, Nanoindentation studies of materials, Materials Today 9 (2006) 32–40.
[47] A. Barnoush, M.T. Welsch, H. Vehoff,Correlation, between dislocation density and pop-in phenomena in aluminum studied by nanoindentation and electron channeling contrast imaging, Scripta Materialia 63 (2010) 465–468.
[48] W.W. Gerberich, J.C. Nelson, E.T. Lilleodden, P. Anderson, J.T. Wyrobek, Indentation induced dislocation nucleation: The initial yield point, Acta Materialia 44 (1996) 3585–3598.
[49] L. Zhang, T. Ohmura, K. Seikido, K. Nakajima, T. Hara, K. Tsuzaki, Direct observation of plastic deformation in iron–3% silicon single crystal by in situ nanoindentation in transmission electron microscopy, Scripta Materialia 64 (2011) 919–922.
[50] P.Z. Berke, T.J. Massart, Computational investigation of slip rate dependent friction as a potential contribution to displacement bursts in nanoindentation of nickel, Tribology International 47 (2012) 167–174.
[51] S.S. Samandari, K.A. Gross,Micromechanical, properties of single crystal hydroxyapatite by nanoindentation, Acta Biomaterialia 5 (2009) 2206–2212.
[52] J. Huang, K. Xu, X.J. Gong, J.F. Wang, Y.M. Fan, J.Q. Liu, X.H. Zeng, G.Q. Ren, T.F. Zhou, H. Yang, Dislocation cross-slip in GaN single crystals under nanoindentation, Applied Physics Letters 98 (2011) 221906–221908.
[53] S. Guicciardi, C. Melandri, F.T. Monteverde, Characterization of Pop-in Phenomena and Indentation Modulus in a Polycrystalline ZrB_2 Ceramic, Journal of the European Ceramic Society 30 (2010) 1027–1034.
[54] N. de la, R. Fox, V.M. Florez, J.A.T. Fernandez, M. Pinero, R.M. Serna, L. Esquivias, Nanoindentation on hybrid organic/inorganic silica aerogels, Journal of the European Ceramic Society 27 (2007) 3311–3316.
[55] L. Chang, L. Zhang, Mechanical behaviour characterisation of silicon and effect of loading rate on pop-in: A nanoindentation study under ultra-low loads, Materials Science and Engineering A 506 (2009) 125–129.
[56] A.B. Mann, J.B. Pethica, W.D. Nix, S. Tomiya, Nanoindentation of epitaxial films: a study of pop-in events. In: Materials research society symposium proceedings, vol. 356, 1994, pp. 271–276.
[57] S.Y. Kuan, X.H. Du, H.S. Chou, J.C. Huang, Mechanical response of amorphous ZrCuTi/PdCuSi nanolaminates under nanoindentation, Surface and Coatings Technology 206 (2011) 1116–1119.
[58] J.J. Roa, E. Jimenez-Pique, T. Puig, X. Obradors, M. Segarra, Nanoindentation of multilayered epitaxial $YBa_2Cu_3O_{7-\delta}$ thin films and coated conductors, Thin Solid Films 519 (2011) 2470–2476.
[59] A. Richter, E. Czerwosz, P. Dłuzewski, M. Kozłowski, M. Nowicki, Nanoindentation of heterogeneous carbonaceous films containing Ni nano-crystals, Micron 40 (2009) 94–98.
[60] J.Y. He, S. Nagao, H. Kristiansen, Z.L. Zhang, Loading rate effects on the fracture of Ni/Au nano-coated acrylic particles, eXPRESS, Polymer Letters 6 (2012) 198–203.
[61] E. Rabkin, J.K. Deuschle, B. Baretzky, On the nature of displacement bursts during nanoindentation of ultrathin Ni films on sapphire, Acta Materialia 58 (2010) 1589–1598.
[62] F. Jose, R. Ramaseshan, A.K. Balamurugan, S. Dash, A.K. Tyagi, B. Raj, Continuous multi cycle nanoindentation studies on compositionally graded $Ti1_{-x}Al_xN$ multilayer thin films, Materials Science and Engineering A 528 (2011) 6438–6444.
[63] P.C. Twigg, F.L. Riley, S.G. Roberts, Nanoindentation investigation of micro-fracture wear mechanisms in polycrystalline alumina, Journal of Materials Science 37 (2002) 845–853.